# Distinguished Author Series

# Overview of Current Hydraulic Fracturing Design and Treatment Technology—Part 2

*by R.W. Veatch, Jr., SPE*

*Ralph Veatch is research supervisor of fracturing at Amoco Production Co. Research Center in Tulsa.* *Part 1 of this paper appeared last month (Pages 677–87) with the author's biography. It addressed stimulation optimization concepts, treatment design considerations, reservoir response potential, fracture propagation, and fracturing rock mechanics.*

*Part 2 is devoted to (1) fracturing materials (fluids, additives, propping agents, etc.), (2) material design (fluid rheology, fluid loss, fracture conductivity, etc.), and (3) field methods to obtain data applicable to predicting and analyzing fracturing behavior.*

## Introduction

Hydraulic fracturing has played a major role in enhancing petroleum reserves and daily production. Fig. 1 portrays a simplified version of the "typical" fracturing process. It consists of blending special chemicals to make the appropriate fracturing fluid, then mixing it with a propping agent (usually sand) and pumping it into the pay zone at sufficiently high rates and pressures that the fluid hydraulically wedges and extends a fracture. At the same time, the fluids carry the proppant deeply into the fracture. When done successfully, the propped open fracture creates a "superhighway" for oil and/or gas to flow easily from the extremities of the formation into the well. Note that the fracture has two wings extending in opposite directions from the well and that it is oriented more or less in the vertical plane. Other types (e.g., horizontal fractures) are known to exist. Some have been observed at relatively shallow depths [<2,000 ft (600 m)], but they comprise a relatively low percentage of the situations experienced to date. Hence, the discussion is directed primarily to vertical fractures.

Fracturing technology requirements are multifaceted and are becoming more complex as our target formations get deeper, hotter, and lower in permeability. Fracturing state of the art over the past decade has changed continually to address the technological challenges that emerged with the development of massive hydraulic fracturing (MHF). This discussion covers much of the currently developing technology and the future needs for technological advances.

0149-2136/83/0051-1922$00.25


## Fracturing Fluids

A fracturing fluid is used basically to: (1) wedge open and extend a fracture hydraulically, and (2) transport and distribute the proppant along the fracture.

The fluid(s) selected for a treatment can have a significant influence on the resulting effectively propped fracture length and fracture conductivity, as well as on the treatment cost. Fluid properties strongly govern fracture-propagation behavior and the distribution and placement of the propping agents. Fluids that leak off rapidly into the formation have a low efficiency in hydraulically wedging and extending a fracture. Fluid leakoff also may leave an undesirable concentration of particulate residue in the fracture that could reduce fracture conductivity. The effective viscosity of the fluid controls the internal fracturing pressure and the propping agent transporting characteristics.

Some desirable features of a fluid for most fracturing treatments include: (1) low fluid loss to obtain the desired penetration with minimum fluid volumes; (2) sufficient effective viscosity to create the necessary fracture width, and to transport and distribute the proppant in the fracture as required; (3) no excessive friction in the fracture; (4) good temperature stability for the particular formation being treated; (5) good shear stability; (6) minimal damaging effects on formation permeability; (7) minimal plugging effects on fracture conductivity; (8) low-friction-loss behavior in the pipe; (9) good post-treatment breaking characteristics; (10) good post-treatment cleanup and flowback behavior; and (11) low cost.

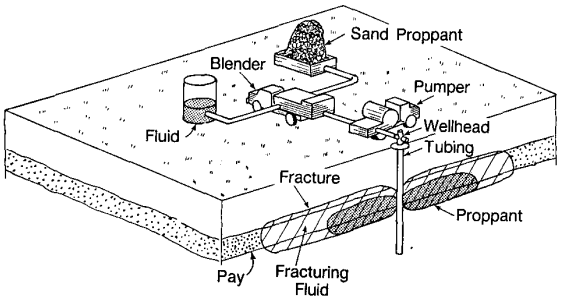


**Fig. 1**—The fracturing process.

**Fluid Systems.** Many different types of fluids currently are available for fracturing treatments. Comprehensive details on all the fluids and their design information are outside the scope of this paper. For any given specific application, one must consult published engineering data or laboratory test data relevant to the conditions to which the fluid is subjected during treatment.

Table 1 lists the various types of fluids or systems generally used today in the U.S. In addition to the basic fluid, there are many additives that perform different functions. Table 2 presents a list of the more common ones.

Major considerations for selecting a system include: (1) formation temperature, fluid temperature profile, and duration of the fluid in the fracture; (2) proposed treatment volume and pumping rates; (3) type of formation (sandstone, limestone, etc.); (4) potential fluid-loss control requirements; (5) formation sensitivity to fluids; (6) reservoir pressure; (7) pumping pressure and pipe-friction limitations; (8) type(s) and quantity of proppant to be pumped; (9) fluid breaking requirements.

Water-base polymers are used in most applications. They cover a wide range of formation types, depths, pressures, temperatures, etc., and are relatively low in cost. Some [guar and hydroxypropyl guar (HPG)] can be crosslinked for added viscosity and an expanded range of temperature application. Temperature stability has been enhanced by addition of oxygen scavengers (e.g., thiosulfate salts, methanol, etc.). Significant fluid-loss enhancement is achieved by addition of 5% dispersed hydrocarbon or by various concentrations and types of solid particulates.

Polymer emulsions generally provide somewhat better fluid-loss behavior, less potential for formation or fracture-conductivity damage, and, in some cases, better proppant transportability. However, they have upper temperature limits on the order of 250°F (121°C). They also can be difficult to break at low temperatures and are somewhat costly.

Gelled hydrocarbons are used primarily on water-sensitive formations, where aqueous fluids invading the fracture face may damage formation permeability. Gelled alcohols also are considered for formations subject to water blockage in the formation pores. Gelled $CO_2$ is claimed to have minimal formation-damage potential with good well flowback characteristics. Gelled acids have proved very effective for stimulating carbonate reservoirs. One problem common to gelled hydrocarbons, alcohols, $CO_2$, or acid systems is that they are usually more costly than water-base polymers.

Aqueous foams usually exhibit very good postfracture cleanup performance when used in stimulating abnormally low-pressured reservoirs or reservoirs that present postfracture cleanup problems

**TABLE 1—COMMONLY USED FRACTURING FLUID SYSTEMS**

| |
|---|
| Water-base polymer solutions of |
| Natural guar gum (guar)* |
| Hydroxypropyl guar (HPG)* |
| Hydroxyethyl cellulose (HEC) |
| Carboxymethyl hydroxyethyl cellulose (CMHEC)* |
| Polymer water-in-oil emulsions |
| 2/3 hydrocarbon** + 1/3 water-base polymer solution† |
| Gelled hydrocarbons |
| Petroleum distillate, diesel, kerosene, crude oil |
| Gelled alcohol (methanol) |
| Gelled $CO_2$ |
| Gelled acid (HCl) |
| Aqueous foams |
| Water phase: guar, HPG solutions |
| Gas phase: nitrogen, $CO_2$ |

*Can be crosslinked to increase viscosity.
**Petroleum distillate, diesel, kerosene, crude oil.
†Usually guar or HPG.

**TABLE 2—TYPICAL FUNCTIONS OR TYPES OF ADDITIVES AVAILABLE FOR FRACTURING FLUID SYSTEMS**

| |
|---|
| Antifoaming agents |
| Bacteria control agents |
| Breakers for reducing viscosity |
| Buffers |
| Clay stabilizing agents |
| Crosslinking or chelating agents (activators) |
| Demulsifying agents |
| Dispersing agents |
| Emulsifying agents |
| Flow diverting or flow blocking agents |
| Fluid-loss control agents |
| Foaming agents |
| Friction reducing agents |
| Gypsum inhibitors |
| pH control agents |
| Scale inhibitors |
| Sequestering agents |
| Sludge inhibitors |
| Surfactants |
| Temperature stabilizing agents |
| Water-blockage control agents |

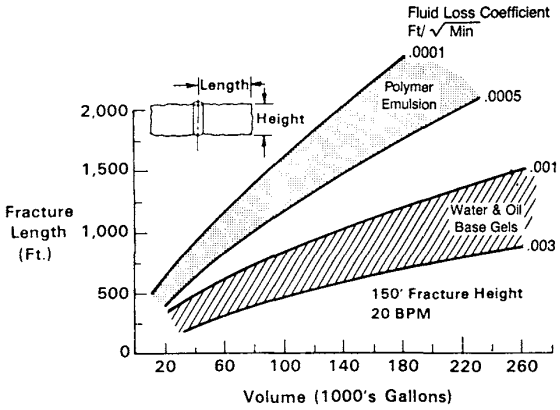


**Fig. 2**—Fluid loss vs. fracture length for low (polymer-emulsion) and high (water- and oil-based gels) fluid-loss behavior.

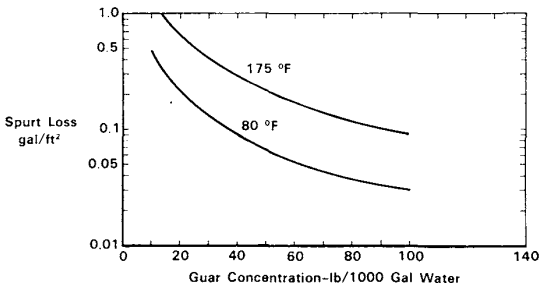


**Fig. 3**—Spurt loss vs. uncrosslinked guar concentration and temperature (formation permeability range = 5 to 10 md).

with denser fracturing fluid systems. Foam systems are becoming more common in current fracturing practices. Because of the gas compressibility at high pressures, applications in deep formations can be costly.

In some instances, stages of different types of fluids may be used in the same treatment. For example, in limestone or dolomite formations one may alternately inject small stages of gelled acid and gelled water. In low-pressure formations it is not uncommon to spearhead a gelled water system with nitrogen, foam, or gelled $CO_2$ to enhance cleanup.

## Fracturing Fluid Design

**Fluid Loss.** Fluid-loss behavior in some cases may have as much effect on fracture penetration as vertical fracture height growth has. Fig. 2 shows the comparative fracture length vs. treatment-volume behavior computed with a hydraulic fracturing simulator for two systems with different fluid-loss behavior. Here, the fluid-loss coefficients used for the polymer-emulsion system calculations were on the order of 0.0001 to 0.0005 ft/min$^{1/2}$ ($0.03\times10^{-3}$ to $0.15\times10^{-3}$ m/min$^{1/2}$). For the water- and oil-based systems, the values ranged from 0.001 to 0.003 ft/min$^{1/2}$ ($0.3\times10^{-3}$ to $0.9\times10^{-3}$ m/min$^{1/2}$). All other parameters used in the calculations were identical. Significantly longer fractures were computed for the more efficient polymer-emulsion system. This demonstrates the impact of fluid loss on a fracturing treatment and the need for reasonably accurate values.

Fluid-loss behavior depends on a number of factors, including (1) type and quantity of gelling agent, (2) type and quantity of fluid-loss additive (FLA), (3) pressure differential between the fracture and the formation, (4) formation permeability and porosity, (5) formation reservoir-fluid flow and compressibility behavior, (6) fracturing fluid and fluid filtrate viscosity/temperature behavior, (7) formation (or fluid) temperature, and (8) the character of any existing natural fractures in the formation.

Total fluid loss generally has two parts: spurt loss and fluid-loss coefficient. Spurt loss pertains to the instantaneous loss when the fluid first is exposed to the fracture face. Fluid-loss coefficient represents long-term behavior over the duration of the exposure. Data in Fig. 3 show that spurt loss is dependent on gel concentration and fluid temperature. It is also somewhat dependent on formation permeability. Spurt loss can be reduced significantly by addition of solid particulate FLA. Many types of these products are available. They usually include one or more of the following materials: silica flour, fine-mesh resin particles, and/or bentonite.

Fluid-loss coefficient usually is represented by three components: $C_I$ (fracturing fluid viscosity and relative permeability effects), $C_{II}$ (reservoir fluid viscosity/compressibility effects), and $C_{III}$ (fracturing fluid wall-building effects). Values for $C_I$ and $C_{II}$ can be computed from rock and fluid properties. Values for $C_{III}$ normally are determined from laboratory tests. Several different methods for computing a combined fluid-loss coefficient, $C$, from $C_I$, $C_{II}$, and $C_{III}$ are discussed by Howard and Fast[1] and Settari.[2] We have yet to determine which method(s) are "most appropriate" for design purposes.

Fig. 4 shows typical wall-building fluid-loss coefficient ($C_{III}$) data. Note the dependence on gel concentration, FLA, and temperature. FLA materials may have significantly different effects in conventional formations from those in tight rocks. Solid particulate FLA may be very effective for a wide range (1 to 150 md) of high- or conventional-permeability formations but is much less effective in tight, low-permeability

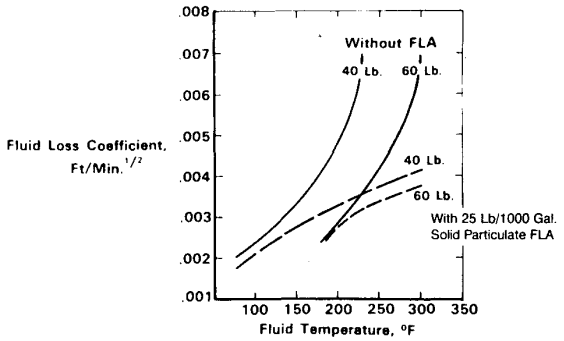


**Fig. 4**—Fluid-loss additives (FLA) and temperature effects on wall-building fluid-loss coefficient ($C_{III}$)—titanate crosslinked 40-lbm (18-kg) and 60-lbm (27-kg) HPG.

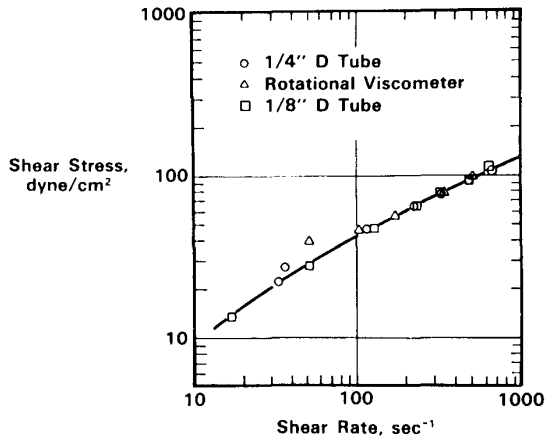


**Fig. 5**—Flow curve for uncrosslinked 40-lbm (18-kg) HPG, 149°F (65°C).

rocks, whereas a 5% hydrocarbon phase dispersed in an HPG system, such as discussed by Penny,[3] can reduce fluid loss significantly in tight formations but have little or no effect in conventional or high-permeability rocks.

Most of the fluid-loss data now available for design, such as shown in Figs. 3 and 4, were obtained from API-type[4] static fluid-loss tests at a pressure differential of 1,000 psi (6.9 MPa). Values may vary with pressure differential. If pressure differentials during fracturing are expected to differ significantly from 1,000 psi (6.9 MPa), consistent laboratory data should be investigated. Fluid-loss behavior under dynamic conditions, as would occur in a fracturing treatment, may be quite different from the implications of static tests. Results published by McDaniel *et al.*,[5] King,[6] Williams,[7] Hall and Dollarhide,[8] and Harris[9] suggest that additional work is necessary to investigate this phenomenon.

**Fluid Rheology.** The wide variety of different types of fracturing fluids is accompanied by wide differences in rheological behavior. Some fluids exhibit a Newtonian flow behavior. Others are non-Newtonian but essentially behave as a power-law fluid. Still others, such as the crosslinked polymers commonly used for MHF treatments, can be very complex, nonpower-law mixtures. For fluids with either a Newtonian or power-law behavior, the rheological design data now available are relatively reliable.

Expressions for rheological behavior are based on the classical power-law fluid relation

$$\tau_w = K\dot{e}_w{}^n, \quad \ldots\ldots\ldots\ldots\ldots\ldots\ldots\ldots\ldots\ldots (1)$$

where

$\tau_w$ = wall shear stress, lbf/sq ft (kPa),
$\dot{e}_w$ = shear rate at the wall, seconds$^{-1}$,
$K$ = consistency index, lbf-sec$^n$/sq ft (kPa·s$^n$), and
$n$ = flow behavior index, dimensionless.

Apparent viscosity, $\mu_a$, is computed by

$$\mu_a = \frac{47{,}880\,K}{\dot{e}_w{}^{(1-n)}}, \quad \ldots\ldots\ldots\ldots\ldots\ldots\ldots\ldots\ldots\ldots (2)$$

where $\mu_a$ is expressed in centipoise.

For power-law fluids, viscous behavior usually is determined per API specifications[4] using a Couette (i.e., coaxial cylinder, bob and rotating sleeve) type viscometer. Rheograms are run to develop flow curves (log-log plots of wall shear stress vs. nominal shear rate, $\dot{e}_c$). Here

$$\dot{e}_c = \frac{2v_\theta}{1-F_r{}^2}, \quad \ldots\ldots\ldots\ldots\ldots\ldots\ldots\ldots\ldots\ldots (3)$$

where $v_\theta$ = relative angular velocity of the bob and sleeve, radians/sec.

$$F_r = r_b/r_s, \quad \ldots\ldots\ldots\ldots\ldots\ldots\ldots\ldots\ldots\ldots (4)$$

where $r_b$ = bob radius, cm, and $r_s$ = sleeve radius, cm.

Slopes and intercepts of the curves are taken to determine values of $n$ and $K_c$, where $K_c$ is related to $K$ by

$$K_c = \left[K\frac{1-F_r{}^2}{n(1-F_r{}^{2/n})}\right]^n \quad \ldots\ldots\ldots\ldots\ldots\ldots (5)$$

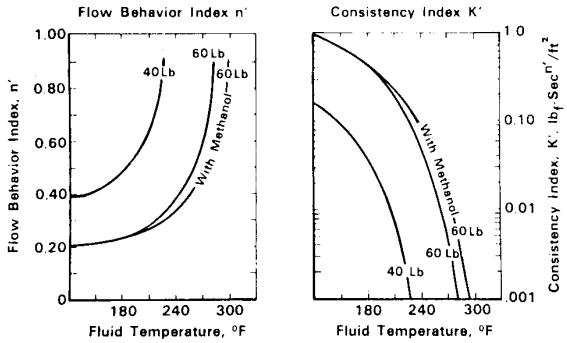


**Fig. 6**—Typical $n'$ and $K'$ behavior—titanate crosslinked 40- and 60-lbm (18- and 27-kg) HPG (2 hours' continuous 170-seconds$^{-1}$ shear at temperature).

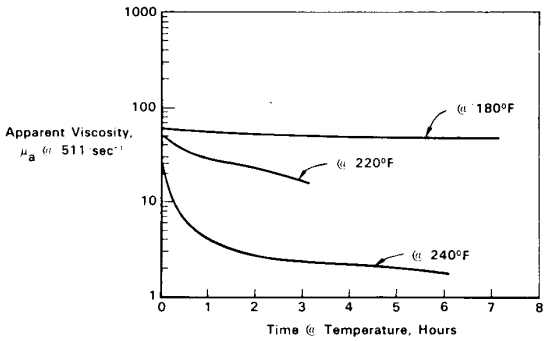


**Fig. 7**—Temperature and time effects on viscosity—40-lbm (18-kg) titanate crosslinked HPG.

at a nominal shear rate $\dot{e}_c = 1.0$. Nominal and wall shear rates are related by

$$\dot{e}_w = \dot{e}_c \left[ \frac{(1-F_r^2)}{n(1-F_r^{2/n})} \right]. \quad \ldots\ldots\ldots\ldots\ldots\ldots (6)$$

For pipe flow, a form commonly used to model rheological behavior is expressed by

$$\frac{d_p \Delta p}{4L} = K_p (8v/d_p)^{n_p}, \quad \ldots\ldots\ldots\ldots\ldots\ldots (7)$$

where

$d_p$ = pipe diameter, ft (m),
$L$ = pipe length, ft (m),
$\Delta p$ = pressure drop, psi (kPa),
$v$ = pipe fluid velocity, ft/sec (m/s),
$n_p$ = $n$ as determined for a power law fluid, and
$8v/d_p$ = apparent shear rate in pipe, seconds$^{-1}$.

$K_p$ is related to $K$ for power-law fluids by

$$K_p = K\left(\frac{3n+1}{4n}\right)^n. \quad \ldots\ldots\ldots\ldots\ldots\ldots (8)$$

For flow in a fracture, rheological behavior customarily is modeled by

$$\frac{b\Delta p}{2x} = K_{f'} (6v_f/b)^{n_{f'}}, \quad \ldots\ldots\ldots\ldots\ldots\ldots (9)$$

where

$x$ = distance along a fracture, ft (m),
$n_{f'}$ = $n$ as determined for a power law fluid,
$b$ = fracture width, ft (m),
$v_f$ = fluid velocity in the fracture, ft/sec (m/s),
$6v_f/b$ = apparent shear rate in the fracture, seconds$^{-1}$, and

$$K_{f'} = K\left(\frac{2n+1}{3n}\right)^n. \quad \ldots\ldots\ldots\ldots\ldots\ldots (10)$$

Even though some fluids do not conform strictly to a power-law behavior, they may follow a "near power-law" behavior sufficiently within some applicable shear-rate range that for practical purposes their behavior can be predicted adequately with an approximated set of $n$ and $K$ values over the given range. One example is shown in Fig. 5. It indicates a slight deviation from power-law behavior in the lower shear-rate range but seems to be "nearly power law" through the major portion of the shear-rate range of interest.

All fracturing fluids exhibit a temperature dependency. The nature and degree depend, of course, on the type of fluid system. For many Newtonian liquids, viscosity can be related to temperature by the Arrhenius relationship,

$$\mu = Fe^{E_a/RT}, \quad \ldots\ldots\ldots\ldots\ldots\ldots\ldots (11)$$

where

$F$ = a thermoviscous constant (characteristic of the fluid),
$E_a$ = activation energy per mole,
$R$ = gas constant,
$T$ = absolute temperature, °R (K),
$\mu$ = Newtonian viscosity, cp (Pa·s), and
$e$ = base of natural logarithms.

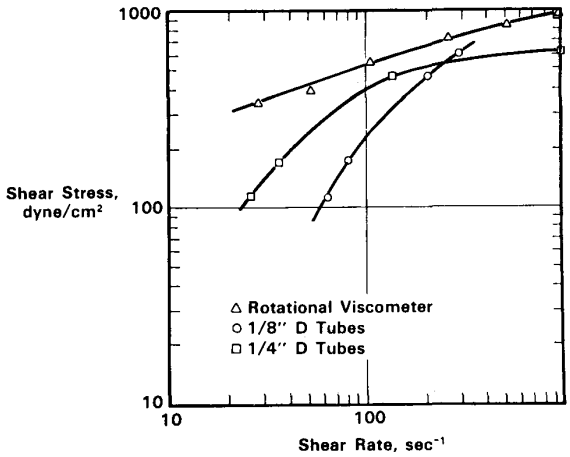


**Fig. 8**—Flow curves from pipe and rotational viscometer—40-lbm (18-kg) crosslinked HPG at 176°F (80°C).

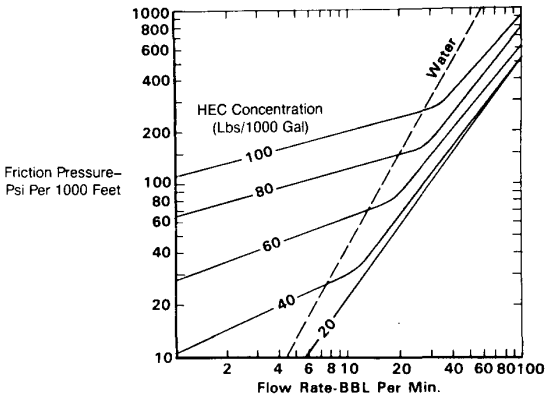


**Fig. 9**—Pipe friction vs. flow rate and gel concentration—HEC/water-based fluids [4½-in. (11.4-cm) OD, 11.6-lbm/ft (17-kg/m) casing].

Eq. 11 may hold for some power-law type and even some nonpower-law fluids such that apparent viscosity behavior follows the relationship over certain temperature ranges. Hence, it is not uncommon to plot log ($\mu_a$) vs. $1/T$ to investigate temperature effects.

Many power-law-type fluids degrade with time and this is accelerated at elevated temperatures. Most of them also show signs of gel degradation at elevated shear. This again depends on the type of system. However, behavior usually can be identified fairly well from a sufficient set of tests over the range of interest.

The crosslinked fluids commonly used in fracturing today because of their purportedly better proppant-carrying and temperature-stability performance have very complex rheological properties. These fluids for the most part are guar or HPG solutions crosslinked with some type of metallic compound (e.g., a borate or titanate compound). The crosslinkers generally are claimed to be unique and proprietary to each fracturing service company. Gel behavior is affected by a number of things, including temperature, temperature history, shear rate and history, time degradation, and chemical contamination. At this time, techniques for characterizing gel rheological behavior are not well established. Flow curves (rheograms) are not always linear and can demonstrate significant dependence on temperature and shear rate. Here, $n$ and $K$ values usually are estimated using a tangent line to the flow curve at a given desired temperature and shear rate to generate sets of data such as shown in Fig. 6. This set is probably unique to the shear-rate (170 seconds$^{-1}$) and time conditions of the test. A variation in either shear rate or time could result in a significantly different set of data. This greatly magnifies the testing requirements to characterize fluid behavior for practical application to fracture design.

Common practice within the industry for crosslinked fluids is to estimate $\mu_a$ with equations developed for power-law fluids (Eq. 2). An example of computed viscosity behavior is given in Fig. 7. This shows the effect of temperature on computed apparent viscosity for a crosslinked HPG fracturing fluid. It can be seen that the fluid degrades with time for a given shear rate and that, for elevated temperatures, the effects of degradation increase drastically.

No accepted standard procedures have been developed to predict behavior of crosslinked fluids or foams accurately. Current problems include repeatability and possibly scaling. An example of this is shown in Fig. 8 from work by Rogers *et al.*[10] This shows comparative Couette and pipe-viscometer data on identical crosslinked fluids. Attempts were made to test the fluids under identical conditions, yet the data did not scale. Reasons for this type behavior are not yet totally resolved. Much additional work is needed to improve rheological characterization methods for fracturing fluids, especially foams and crosslinked fluids. Recent work presented by several investigators[11-17] addresses some needs in this area.

**Pipe-Flow Data.** Fig. 9 illustrates typical pipe-flow data available for a wide range of pipe configurations. This set shows both the laminar ($m \approx ½$ cycle/cycle) and turbulent ($m \approx 1½$ cycle/cycle) regime for various HEC gel concentrations in 4½-in. (11.4-cm) casing. Experience has indicated excellent agreement between design data and field practice for uncrosslinked fluids. However, with crosslinked fluids, variations in the crosslinking mechanism at different points in the pipe while pumping can create fluctuations in friction

**TABLE 3—API FRACTURING-SAND-SIZE DESIGNATION**

| Mesh Range Designation | Size ($\mu$m) |
|---|---|
| Primary Sizes | |
| 12/20 | 850 to 1,700 |
| 20/40 | 425 to 850 |
| 40/70 | 212 to 425 |
| Alternate Sizes | |
| 6/12 | 1,700 to 3,350 |
| 8/16 | 1,180 to 2,360 |
| 16/30 | 600 to 1,180 |
| 30/50 | 300 to 600 |
| 70/140 | 106 to 212 |

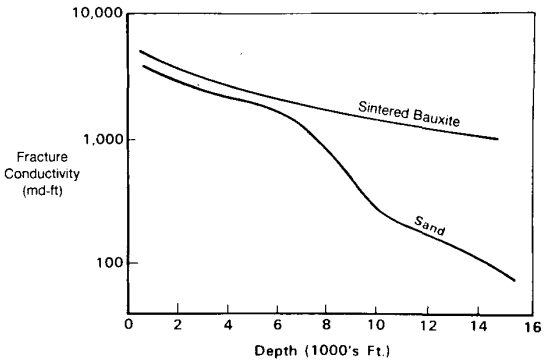


**Fig. 10**—Expected typical fracture conductivity vs. depth [closure stress gradient = 0.7-psi/ft (15.4-kPa/m) depth].

pressure. Such fluctuations have been observed from downhole treating pressure measurements on MHF jobs.

### Propping Agents

The function of a propping agent (proppant) is to hold the fracture open after the hydraulic treatment has been completed. The reservoir fluids then can flow through the conductive path created by the proppant pack in the fracture.

Silica sand is by far the most commonly used proppant in the U.S. today. The ready availability and low cost of high-quality sands that can provide good fracture conductivity for a wide range of conditions make them very attractive for fracture stimulation. API has established sand-quality specifications for use in fracturing treatments.[18] These basically cover size distribution, sphericity and roundness, solubility in acid, silt and clay content, and crush resistance. The size designations for fracturing sands are given in Table 3. They relate to the corresponding-size openings of sieves used in processing the sands. The remainder of the specifications are described in Ref. 18.

Another material now in common use is sintered bauxite (aluminum oxide). It is significantly stronger than sand and is used in deep formations where high fracture-closure stresses severely crush sand. High-strength glass beads were commonly used in the past but recently have been replaced by sintered bauxite for deep applications.

Fig. 10 compares fracture conductivity vs. depth (i.e., closure stress) for sand and sintered bauxite. This illustrates the improvement that can be achieved with sintered bauxite in deeper formations. This is especially pronounced at depths below 10,000 ft (3000 m), where high stresses begin to crush sand. However, sintered bauxite has one definite disadvantage—it has a much higher density than sand. With a specific gravity of 3.5 to 3.7 compared with 2.65 for sand, sintered bauxite is not transported as easily by fracturing fluids.

A variety of materials, including alumina, cordierite, mullite, silicon carbide, and some ceramic oxides,[19-22] currently are being investigated for use as proppants. Certain ceramics are being developed commercially to serve an intermediate strength requirement between sand and sintered bauxite. Zirconium oxide is available from Europe as an alternative to sintered bauxite, but it has just recently entered the U.S. market. Coated proppants[23] (i.e., sand coated with a polymeric material) also are being introduced. One purpose of the coating is to relieve high stresses caused by grain-to-grain contact and thus to improve the load-carrying capacity of the proppant pack. Coated proppants have not yet been used extensively enough to evaluate their overall effectiveness.

**Fracture Conductivity.** To estimate fracture-conductivity values that may be expected from a proppant, these things should be considered: (1) type of proppant, (2) proppant size distribution, (3) proppant concentration in the fracture, (4) stress load on the proppant pack, (5) formation embedment characteristics, and (6) potential plugging from fracturing fluid residue.

Fracture-conductivity laboratory flow tests performed in radial or linear flow cells with the proppant subjected to a fracture-simulated load are used to develop design data as shown in Fig. 11.[24] This shows fracture conductivity of 20-/40-mesh sand for a wide variety of closure stresses and sand concentrations in the fracture. The peaks in fracture conductivity at concentrations around 100 lbm/1,000 sq ft (0.49 kg/m$^2$) reflect the existence of a partial monolayer. As sand concentration increases to a fully packed monolayer in the 200- to 400-lbm/1,000 sq ft (0.98- to 1.9-kg/m$^2$) range, conductivity declines. The increase for concentrations above 500 lbm/1,000 sq ft

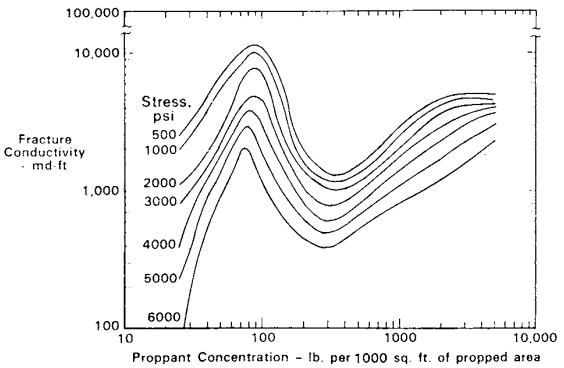


**Fig. 11**—Fracture conductivity, closure stress, and proppant concentration—20/40 fracturing sand (Ref. 25).

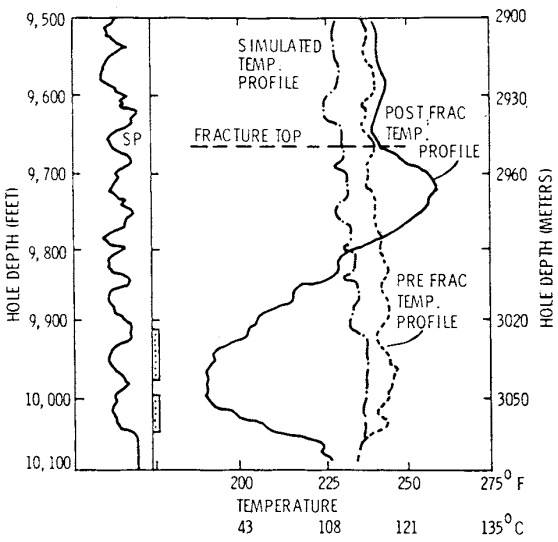


**Fig. 12**—Temperature profiles: prefracture, postfracture (PFTDP), and prefracturing model simulated.

(2.4 kg/m$^2$) results from the multiple proppant layers in wider fractures. In most fracture designs, it is advisable to try to achieve concentrations of at least 1 lbm/sq ft (4.9 kg/m$^2$). In vertical fractures, where proppants can fall to lower parts of the fracture, it may be extremely difficult to design a treatment guaranteed to achieve a partial monolayer. Another problem usually associated with monolayers is proppant embedment in the formation. For soft formations where embedment is severe, fracture conductivities of partial or full monolayers can be much lower than Fig. 11 shows.

The preceding comments have not addressed the possibility of a reduction in fracture conductivity resulting from partial plugging by fracturing-fluid residue. As discussed by Cooke[25] and Almond,[26] this sometimes can have a significant effect. Hence, we may need to resort to laboratory data to investigate potential effects for particular situations.

## Fracture Design Data From Field Experience

The results of a number of field data-collection programs to investigate methods for improving fracture design capabilities have been reported by Veatch and Crowell.[27] The programs have improved our ability to obtain better estimates of $C$, $E$, net fluid-loss interval ($h_\ell$), fracture-height growth behavior [$h_f(p_n)$], critical net fracturing pressure ($p_{n'}$), fracture closure stress ($p_c$), and fracture extension pressure ($p_f$), which often are essential for fracture design. In addition, the knowledge of downhole fracturing pressure behavior has added a new dimension to design technology. This has provided significant insight into methods for controlling undesirable vertical fracture growth and for designing fluid and proppant schedules to improve fracture conductivity. In view of this, some highlights of these programs are summarized here.

**Fracture Height Measurement.** Postfracturing temperature-decay profile (PFTDP) surveys currently are one of the most widely applicable techniques for determining fracture height at the wellbore. However, interpretation sometimes is masked by temperature anomalies usually in the form of a "warm nose" as depicted near the 9,700-ft (2960-m) depth mark in Fig. 12. The use of post-water-circulation temperature-decay surveys taken before perforating can significantly improve the interpretation of PFTDP data for fracture height. As shown in Fig. 12, the prefracture surveys serve as a baseline for temperature behavior where no fluid has entered the formation. The procedures and results from many of the early tests were reported by Dobkins.[28] Subsequent tests[27] have strengthened his conclusions.

One possible cause of the warm nose may be warmed fluid in the fracture flowing back past the wellbore from one portion of the fracture to another after pumping has ceased at the end of the fracturing job. It is postulated that continued fracture extension at one or more points in the fracture after shut-in can cause a redistribution of fluid in the fracture carrying heat back across the wellbore after shut-in, causing the warm nose to develop.

Radioactive surveys run with PFTDP surveys after fracturing also have been found to enhance fracture height interpretation. They can be especially helpful to assist confirmation of fracture height when the warm nose appears on the PFTDP surveys. They also are very effective for investigating the bottom of the fracture. Sand fill in the wellbore sometimes precludes this for PFTDP surveys.

**Downhole Fracturing Pressure (DFP).** Procedures and findings from early tests were discussed by Nolte

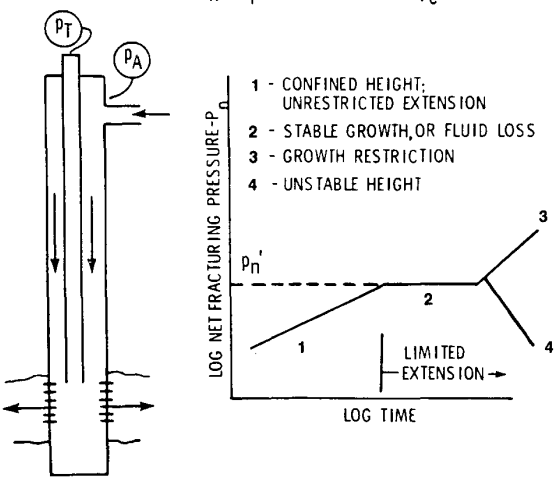


**Fig. 13**—Wellbore net fracturing pressure behavior during treatment—vertically confined fractures.

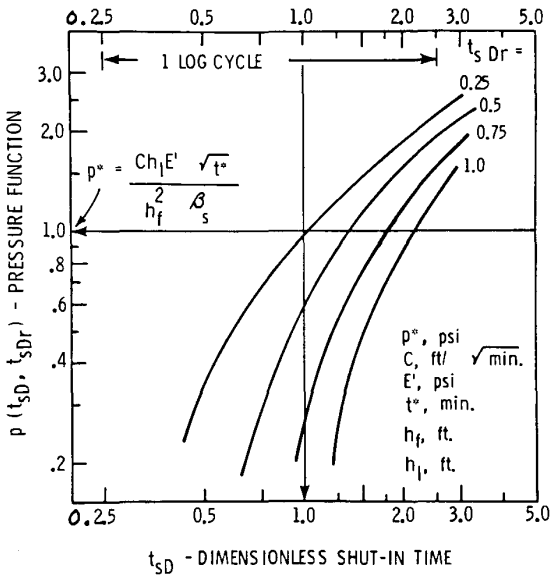


**Fig. 14**—Postfracturing treatment shut-in pressure master decline (PFPD) type curves.

and Smith.[29] Many subsequent tests [27] have confirmed their observations. Lateral fracture extension rates, critical net fracturing pressures, and vertical growth behavior can be inferred from DFP data. This is depicted conceptually in Fig. 13 by a logarithmic plot of net fracturing pressure ($p_n$) vs. time. Here, Mode 1 ($m \approx 1/8$ to 1/4) indicates confined height and free lateral-fracture extension. This is consistent with the expression

$$p \sim \frac{(E^3 \mu q_i x_f)^{1/4}}{h_f} \quad \ldots\ldots\ldots\ldots\ldots\ldots\ldots\ldots (12)$$

suggested by Nolte and Smith (Eq. 7 in Part I of this paper).

Mode II ($m \approx 0$) indicates a reduced fracture-penetration rate. Here the pressure remains essentially constant at some $p_{n'}$ value. One of several possible explanations for this is that side fissures take fluid from the main fracture. Another possible explanation is the occurrence of stabilized low-rate vertical fracture growth. In some formations the $p_{n'}$ values may not change much from well to well; in others they may vary quite a bit. This knowledge is valuable for design purposes. Mode III ($m \geq 1$) can be interpreted as a storage mode with restricted vertical or lateral extension and implied "ballooning" width. Mode IV ($m < 0$) indicates rapid vertical growth.

**Postfracturing Pressure Decline (PFPD).** Numerous design parameters can be inferred from pressure decline following the instantaneous shut-in pressure. These include $p_c$, $h_\ell$, $C$, $E$, $h_f$, and $x_f$. Development and application of the theory and type-curve techniques for PFPD data obtained during the initial portion of the program were presented by Nolte.[30] Procedures for analysis, using the pressure-decline master type curve shown in Fig. 14, are documented in Ref. 30. This can be particularly useful with a minifracturing calibration test (discussed later) to obtain $C$, $E$, $H_\ell$, $p_c$, and $p_f$ values on a given well before MHF for use in designing its treatment.

PFPD data are very easy and relatively inexpensive to obtain. They do not require high-resolution pressure-measuring equipment [accuracy of $\pm 10$ psi ($\pm 68.9$ kPa) will yield satisfactory results]. They involve merely leaving a pressure-recording chart connected to the well for a shut-in period of usually two to three times the length of the pumping period.

**Minifracturing Calibration (MFC) Tests.** These are aimed at measuring pertinent data directly on a well before designing the MHF treatment. They can yield excellent values of $p_c$, $p_f$, and $C$ and some indication of the $E/h_f$ ratio. Analysis of these pressure data can imply an expected $h_f(p_n)$ relationship during MHF. The program may be conducted along with routine perforation breakdown operations before flow testing.

First, a closure stress test to obtain $p_c$ and/or $p_f$ is conducted during perforation breakdown using conventional nondamaging breakdown fluids (KCl water, acids, etc.). The procedure may include conventional step-rate tests, repeated pump-

**TABLE 4—COMPARISON OF FLUID-LOSS COEFFICIENT VALUES OBTAINED FROM FIELD TESTS VS. LABORATORY MEASUREMENTS**

| Formation | Permeability ($\mu$d) | Fluid Type* | Field Data ($10^{-3}$ ft/min$^{1/2}$) | Laboratory Data ($10^{-3}$ ft/min$^{1/2}$) |
|---|---|---|---|---|
| Cotton Valley (TX) | 1 to 100 | 1, 2, 4 | 0.3 to 0.7 | 0.7 to 1.0 |
| Muddy J (CO) | 1 to 100 | 1, 3 | 0.5 to 0.7 | 0.3 to 0.7 |
| Frontier (WY) | 1 to 300 | 1, 2 | 1.0 to 1.2 | 1.0 to 1.5 |
| Mesa Verde (WY) | 1 to 100 | 1, 2 | 1.0 to 6.0 | 0.5 to 2.0 |
| Dakota (NM) | 10 to 1,000 | 1, 2 | 0.8 to 1.2 | 1.0 to 1.5 |

*1 = 40 or 50 lbm gel/1,000 gal crosslinked HPG.
2 = 1 plus 5% hydrocarbon.
3 = polymer emulsion.
4 = 50 lbm gel/1,000 gal crosslinked cellulose derivative.

in/flowback operations with small fluid volumes [e.g., 100 to 5,000 gal (0.37 to 18.9 m$^3$)], and shut-in pressure-decline tests. An MFC test then is performed using moderate volumes [e.g., 5,000 to 20,000 gal (18.9 to 75.6 m$^3$)] of the same fracturing fluid anticipated for use throughout the major portion of the MHF treatment. This fluid must be proppant-free to allow the fracture to close unrestricted. DFP is recorded while pumping, and PFPD data are taken following shut-in. During this shut-in period, PFTDP surveys are taken to measure $h_f$.

These tests have been found to yield a good calibration of the formation. In some cases it also may be possible to infer $p_{n'}$ values and $h_f(p_n)$ behavior from the data. This approach is especially effective for investigating static in-situ $C$ values for the fracturing fluid anticipated for the treatment. This, of course, requires an estimate of $h_f$ and $h_\ell$. Table 4 shows a comparison of MFC-calculated $C$ values vs. laboratory data.

**In-Situ Stress and Rock Property Measurement.** This involves methods for estimating in-situ stresses and mechanical rock properties from downhole wireline devices. Methods to date primarily have centered on the use of acoustical surveys to acquire compressional and shear-wave data for correlation with measured closure pressures and laboratory-measured $E$ values and Poisson's ratios ($\nu$). Preliminary findings in the east Texas Cotton Valley were reported by Rosepiler.[31] These showed that in-situ principal stress values were stratified vertically in that area and that indications of this could be inferred from downhole surveys.

However, routine methods for quantifying in-situ stress and rock properties using readily available commercial equipment and services are still being evaluated. The prospects of applying new tools such as those discussed by Voegele and Jones,[32] Fertl,[33] Koerperich,[34] and Aron and Murray[35] appear encouraging.

**Fracture Azimuth Mapping Methods.** These encompass investigation methods for measuring fracture azimuth, symmetry, and lateral growth-rate behavior created by MHF treatments. This knowledge is extremely important in very tight formations where well locations should be selected to minimize interference of the long fractures. A full complement of tests was run in the 8,000-ft (2400-m) deep Wattenberg area in Colorado. Refs. 36 through 39 present details of the equipment, procedures, and findings. Results were encouraging.

Subsequent tests in deeper horizons in Wyoming [11,000 ft (3300 m)] and Texas [10,000 ft (3000 m)] have been more questionable than those from Wattenberg. Thus, the potential of using tiltmeters may have some depth limitations. However, other methods, including borehole directional geophone measurements, earth tidal strain data,[40] rock mechanics data from oriented cores,[41] borehole ellipticity data, and magnetometer measurements,[42] may provide means for measuring or inferring azimuth.

## Use of Data in Fracturing Treatment Design

As stated in Part 1, the requirements for fracture design data may vary widely from one field to another. In some fields, "ballpark" estimates may suffice; in others, this may be fatal. The same is true for fracturing-simulation models. Different areas may require different degrees of sophistication. The previous discussion indicated that many design parameters are not constant and may vary significantly throughout a treatment. Simpler models use mostly constant parameter values for input. More complex simulators can account for variations in behavior. One should investigate the effects that may result from variations in behavior to determine the required level of simulation sophistication. If conditions are such that the parameters do not vary significantly, then simplified methods like those presented by McLeod[43] may provide very adequate treatment designs. However, if, for example, vertical growth or fluid viscosity changes significantly during the course of a treatment, a model that accounts for this should be used.

## Conclusions

Fracturing technology and our abilities to design and

perform treatments are continuing to improve. Progress over the past decade has turned some previously "dry" prospects into commercial plays, and the results of the industry effort have been very encouraging. However, the challenges have not abated. Significant advances still are needed for economical development of very deep or very hot reservoirs, lenticular formations, and many of the unconventional resources (tight gas or oil formations, hydrocarbon-bearing shales and/or coals, etc.).

## Nomenclature

$b$ = fracture width, ft (m)
$C$ = combined fluid-loss coefficient, ft/min$^{1/2}$ (m/min$^{1/2}$)
$C_{\mathrm{I}}$ = fluid-loss coefficient, effects of fracturing fluid viscosity and relative permeability, ft/min$^{1/2}$ (m/min$^{1/2}$)
$C_{\mathrm{II}}$ = fluid-loss coefficient, effects of reservoir fluid viscosity/compressibility, ft/min$^{1/2}$ (m/min$^{1/2}$)
$C_{\mathrm{III}}$ = fluid-loss coefficient, wall building effects, ft/min$^{1/2}$ (m/min$^{1/2}$)
$d_p$ = pipe diameter, in. (cm)
$D$ = depth, ft (m)
$e$ = base of natural logarithms
$\dot{e}_c$ = nominal shear rate, seconds$^{-1}$
$\dot{e}_w$ = shear rate at wall, seconds$^{-1}$
$E$ = Young's modulus of elasticity
$E'$ = plane strain modulus$=E/(1-\nu^2)$
$E_a$ = fluid activation energy per mole
$F$ = thermoviscous constant characteristic of a fluid
$F_r$ = viscometer bob/sleeve radius ratio$=r_b/r_s$
$h$ = formation net pay, ft (m)
$h_f$ = fracture height, ft (m)
$h_\ell$ = net fluid loss height, ft (m)
$K, K_c, K_f, K_p$ = consistency index, lbf-sec/sq ft (Pa·s)
$L$ = pipe length, ft (m)
$m$ = slope
$n, n_p, n_f$ = flow behavior index
$p$ = pressure, psi (Pa)
$p_A$ = surface annulus pressure, psi (Pa)
$p_c$ = fracture closure pressure (wellbore), psi (kPa)
$p_f$ = fracture extension pressure, psi (kPa)
$p_n$ = net fracturing pressure (wellbore) $=(p-p_c)$, psi (kPa)
$p_{n'}$ = critical net fracturing pressure—i.e., pressure capacity (wellbore), psi (kPa)
$p_T$ = surface tubing pressure, psi (kPa)
$p^*$ = postfracturing pressure-decline type curve match, psi (kPa)
$\Delta p$ = pressure drop, psi/ft (kPa/m)
$q_i$ = injection rate, bbl/min (m$^3$/s)
$r_b$ = viscometer bob radius, cm
$r_s$ = viscometer sleeve radius, cm
$R$ = gas constant
$t^*$ = pumping time, minutes
$t_{sD}$ = postfracturing dimensionless shut-in time$=\Delta t/t^*$
$t_{sDr}$ = reference shut-in time for pressure differences, minutes
$\Delta t$ = time since shut-in, hours
$T$ = temperature, °R (K)
$v$ = pipe fluid velocity, ft/sec (m/s)
$v_f$ = fluid velocity in a fracture, ft/sec (m/s)
$v_\theta$ = relative angular velocity of viscometer bob and sleeve, radians/sec
$x$ = distance from the wellbore to some point in a fracture, ft (m)
$x_f$ = fracture length, ft (m)
$\beta_s$ = ratio of average and wellbore fracture pressures while shut in
$\mu$ = viscosity, cp (Pa·s)
$\mu_a$ = apparent viscosity, cp (Pa·s)
$\nu$ = Poisson's ratio
$\tau_w$ = wall shear stress, lbf/sq ft (kPa)

## References


1. Howard, G.C. and Fast, C.R.: *Hydraulic Fracturing*, Monograph Series, SPE, Dallas (1970) **2.**
2. Settari, A.: "A New General Model of Fluid Loss in Hydraulic Fracturing," paper SPE 11625 presented at the 1983 SPE/DOE Low-Permeability Gas Reservoirs Symposium, Denver, March 13–16.
3. Penny, G.S.: "Nondamaging Fluid-Loss Additives for Use in Hydraulic Fracturing of Gas Wells," paper SPE 10659 presented at the 1982 SPE Formation Damage Control Symposium, Lafayette, March 24–25.
4. "Recommended Practice for Standard Procedures for the Evaluation of Hydraulic Fracturing Fluids," RP 39, API, Dallas (1983).
5. McDaniel, R.R., Deysarkar, A.K., and Callanan, M.J.: "An Improved Method for Measuring Fluid Loss at Simulated Fracture Conditions," paper SPE 10259 presented at the 1981 SPE Annual Technical Conference and Exhibition, San Antonio, Oct. 4–7.
6. King, G.E.: "Factors Affecting Dynamic Fluid Leakoff With Foam Fracturing Fluids," paper SPE 6817 presented at the 1977 SPE Annual Technical Conference and Exhibition, Denver, Oct. 9–12.
7. Williams, B.B.: "Fluid Loss From Hydraulically Induced Fractures," *Trans.*, AIME (1970) **249**, 882–88.
8. Hall, C.D. Jr. and Dollarhide, F.E.: "Fracturing Fluid-Loss Agent Performance Under Dynamic Conditions," *J. Pet. Tech.* (July 1968) 763–68.
9. Harris, P.C.: "Dynamic Fluid-Loss Characteristics of Foam Fracturing Fluids," paper SPE 11065 presented at the 1982 SPE Annual Technical Conference and Exhibition, New Orleans, Sept. 26–29.
10. Rogers, R.E., Veatch, R.W., and Nolte, K.G.: "Pipe Viscometer Study of Fracturing Fluid Rheology," paper SPE 10258 presented at the 1981 SPE Annual Technical Conference and Exhibition, San Antonio, Oct. 4–7.

11. Cloud, J.E. and Clark, P.E.: "Stimulation Fluid Rheology III. Alternatives to the Power Law Fluid Model for Crosslinked Gels," paper SPE 9332 presented at the 1980 SPE Annual Technical Conference and Exhibition, Dallas, Sept. 21-24.
12. Ainley, B.R. and Charles, G.J.: "Fracturing Using a Stabilized Foam Pad," paper SPE 10825 presented at the 1982 SPE/DOE Unconventional Gas Recovery Symposium, Pittsburgh, May 16-18.
13. Lescarboura, J.A., Sifferman, T.R., and Wahl, H.A.: "Evaluation of Fracturing Fluid Stability Using a Heated Pressurized Flow Loop," paper SPE 10962 presented at the 1982 SPE Annual Technical Conference and Exhibition, New Orleans, Sept. 26-29.
14. Conway, M.W., and Harris, L.W.: "A Laboratory and Field Evaluation of a Technique for Hydraulic Fracturing Stimulation of Deep Wells," paper SPE 10964 presented at the 1982 SPE Annual Technical Conference and Exhibition, New Orleans, Sept. 26-29.
15. Gardner, D.C. and Eikerts, J.V.: "The Effects of Shear and Proppant on the Viscosity of Crosslinked Fracturing Fluids," paper SPE 11066 presented at the 1982 SPE Annual Technical Conference and Exhibition, New Orleans, Sept. 26-29.
16. Baumgartner, S.A. *et al.*: "High-Efficiency Fracturing Fluids for High-Temperature, Low-Permeability Reservoirs," paper SPE 11615 presented at the 1983 SPE/DOE Low-Permeability Gas Reservoirs Symposium, Denver, March 13-16.
17. Craigie, L.J.: "A New Method for Determining the Rheology of Crosslinked Fracturing Fluids Using Shear History Simulation," paper SPE 11635 presented at the 1983 SPE/DOE Low-Permeability Gas Reservoirs Symposium, Denver, March 13-16.
18. "Recommended Practices for Testing Sand Used in Hydraulic Fracturing Operations," RP 56, API, Dallas (1983).
19. Cutler, R.A. *et al.*: "New Proppants for Deep Gas Well Stimulation," paper SPE 9869 presented at the 1981 SPE/DOE Low-Permeability Gas Reservoirs Symposium, Denver, May 27-29.
20. Neal, E.A., Parmley, J.L., and Colpays, P.J.: "Oxide Ceramic Proppants for Treatment of Deep Well Fractures," paper SPE 6816 presented at the 1977 SPE Annual Technical Conference and Exhibition, Denver, Oct. 9-12.
21. Callanan, M.J., McDaniel, R.R., and Lewis, P.E.: "Application of a New SEcond-Generation High-Strength Proppant in Tight Gas Reservoirs," paper SPE 11633 presented at the 1983 SPE/DOE Low Permeability Gas Reservoirs Symposium, Denver, March 13-16.
22. Cutler, R.A., *et al.*: "Comparison of the Fracture Conductivity of Commercially Available and Experimental Proppants at Intermediate and High Closure Stresses," paper SPE 11634 presented at the 1983 SPE/DOE Low Permeability Gas Reservoirs Symposium, Denver, March 13-16.
23. Sinclair, A.R., and Graham, J.W.: "A New Proppant for Hydraulic Fracturing," paper presented at the 1978 ASME Energy Technology Conference, Houston, Nov. 5-9.
24. "The Fracbook™ Design/Data Manual for Hydraulic Fracturing," Halliburton Services, Duncan, OK (1971).
25. Cooke, C.E. Jr.: "Effects of Fracturing Fluid on Fracture Conductivity," *J. Pet. Tech.* (Oct. 1975) 1273-82.
26. Almond, S.W.: "Factors Affecting Gelling-Agent Residue Under Low Temperature Conditions," paper SPE 10658 presented at the 1982 SPE Formation Damage Control Symposium, Lafayette, March 24-25.
27. Veatch, R.W. Jr. and Crowell, R.F.: "Joint Research Operations Programs Accelerate Massive Hydraulic Fracturing Technology," *J. Pet. Tech.* (Dec. 1982) 2763-75.
28. Dobkins, T.A.: "Improved Methods To Determine Hydraulic Fracture Height," *J. Pet. Tech.* (April 1981) 719-26.
29. Nolte, K.G. and Smith, M.B.: "Interpretation of Fracturing Pressures," *J. Pet. Tech.* (Sept. 1981) 1767-75.
30. Nolte, K.G.: "Determination of Fracturing Parameters from Fracturing Pressure Decline," paper SPE 8341 presented at the 1979 SPE Annual Technical Conference and Exhibition, Las Vegas, Sept. 23-26.
31. Rosepiler, M.H.: "Determination of Principal Stresses and the Confinement of Hydraulic Fractures in Cotton Valley," paper SPE 8405 presented at the 1979 SPE Annual Technical Conference and Exhibition, Las Vegas, Sept. 23-26.
32. Voegele, M.D. and Jones, A.H.: "A Wireline Hydraulic Fracturing Tool for Determination of In-Situ Stress Contrasts," paper SPE 8937 presented at the 1980 SPE/DOE Unconventional Gas Recovery Symposium, Pittsburgh, May 18-20.
33. Fertl, W.H.: "Evaluation of Fractured Reservoir Rocks Using Geophysical Well Logs," paper SPE 8938 presented at the 1980 SPE/DOE Unconventional Gas Recovery Symposium, Pittsburgh, May 18-20.
34. Koerperich, E.A.: "Shear-Wave Velocities Determined From Long- and Short-Spaced Borehole Acoustical Devices," *Soc. Pet. Eng. J.* (Oct. 1980) 317-26.
35. Aron, J. and Murray, J.: "Formation Compressional and Shear Interval Transit-Time Logging by Means of Long Spacings and Digital Techniques," paper SPE 7446 presented at the 1978 SPE Annual Technical Conference and Exhibition, Houston, Oct. 1-4.
36. Smith, M.B., *et al.*: "The Azimuth of Deep Penetrating Fractures in the Wattenberg Field," *J. Pet. Tech.* (Feb. 1978) 185-93.
37. Smith, M.B., Logan, J.M., and Wood, M.D.: "Fracture Azimuth—A Shallow Experiment," *Trans.*, ASME (June 1980) **102**, 99-105.
38. Wood, M.D., Pollard, D.D., and Raleigh, C.B.: "Determination of In-Situ Geometry of Hydraulically Generated Fractures Using Tiltmeters," paper SPE 6091 presented at the 1976 SPE Annual Technical Conference and Exhibition, New Orleans, Oct. 3-6.
39. Schuster, C.L.: "Detection Within the Wellbore of Seismic Signals Created by Hydraulic Fracturing," paper SPE 7448 presented at the 1978 SPE Annual Technical Conference and Exhibition, Houston, Oct. 1-4.
40. Hanson, J.M. and Owen, L.B.: "Fracture Orientation Analysis by the Solid Earth Tidal Strain," paper SPE 11070 presented at the SPE 1982 Annual Technical Conference and Exhibition, New Orleans, Sept. 26-29.
41. Clark, J.A.: "Prediction of Hydraulic Fracture Azimuth Through Geological, Core, and Analytical Studies," paper SPE 11611 presented at the 1983 SPE/DOE Low-Permeability Gas Reservoirs Symposium, Denver, March 13-16.
42. Wood, M.D. *et al.*: "Fracture Proppant Mapping Using Surface Superconducting Magnetometers," paper SPE 11612 presented at the 1983 SPE/DOE Low Permeability Gas Reservoirs Symposium, Denver, March 13-16.
43. McLeod, H.O. Jr.: "A Simplified Approach to Design of Fracturing Treatments Using High-Viscosity Crosslinked Fluids," paper SPE 11614 presented at the 1983 SPE/DOE Low Permeability Gas Reservoirs Symposium, Denver, March 13-16.


## SI Metric Conversion Factors

| | | | | |
|---|---|---|---|---|
| bbl | × 1.589 873 | E−01 | = | $m^3$ |
| dyne/$cm^2$ | × 1.0* | E−01 | = | Pa |
| ft | × 3.048* | E−01 | = | m |
| °F | (°F−32/1.8) | | = | °C |
| gal | × 3.785 412 | E−03 | = | $m^3$ |
| in. | × 2.54* | E+00 | = | cm |
| lbf | × 4.448 222 | E+00 | = | N |
| lbm | × 4.535 924 | E−01 | = | kg |
| psi | × 6.894 757 | E−03 | = | MPa |
| sq ft | × 9.290 304 | E−02 | = | $m^2$ |

*Conversion factor is exact.

**JPT**

**Distinguished Author Series** articles are general, descriptive presentations that summarize the state of the art in an area of technology by describing recent developments for readers who are not specialists in the topics discussed. Written by individuals recognized as experts in the areas, these articles provide key references to more definitive work and present specific details only to illustrate the technology. **Purpose:** To inform the general readership of recent advances in various areas of petroleum engineering. The series is a project of the Technical Coverage Committee.